Talanta 125 (2014) 14–23

Contents lists available at ScienceDirect

Talanta

journal homepage: www.elsevier.com/locate/talanta

A simple and sensitive surface molecularly imprinted polymers based fluorescence sensor for detection of λ-Cyhalothrin

Chunbo Liu [a,*], Zhilong Song [a], Jianming Pan [a,*], Yongsheng Yan [a], Zhijing Cao [a], Xiao Wei [b], Lin Gao [a], Juan Wang [a], Jiangdong Dai [b], Minjia Meng [a], Ping Yu [a]

[a] School of Chemistry and Chemical Engineering, Jiangsu University, Zhenjiang 212013, China
[b] School of Material Science and Engineering, Jiangsu University, Zhenjiang 212013, China

ARTICLE INFO

Article history:
Received 2 December 2013
Received in revised form
21 February 2014
Accepted 24 February 2014
Available online 5 March 2014

Keywords:
Surface molecular imprinted
λ-Cyhalothrin
Detection
Fluorescent
Quenching

ABSTRACT

In this study, surface molecularly imprinted $YVO_4:Eu^{3+}$ nanoparticles with molecular recognitive optosensing activity were successfully prepared by precipitation polymerization using λ-Cyhalothrin (LC) as template molecules, methacrylic acid and ethylene glycol dimethacrylate as the polymerization precursors which could complex with template molecules, and the material has been characterized by SEM, TEM, FT-IR, XRD, TGA and so on. Meanwhile, the as-prepared core–shell structured nanocomposite ($YVO_4:Eu^{3+}$@MIPs), which was composed of lanthanide doped $YVO_4:Eu^{3+}$ as fluorescent signal and surface molecular imprinted polymers as molecular selective recognition sites, could selectively and sensitively optosense the template molecules. After the experimental conditions were optimized, two linear relationship were obtained covering the concentration range of 2.0 – 10.0 μM and 10.0 – 90.0 μM, and the limit of detection (LOD) for LC was found to be 1.76 μM. Furthermore, a possible mechanism was put forward to explain the fluorescence quenching of $YVO_4:Eu^{3+}$@MIPs. More importantly, the obtained sensor was proven to be suitable for the detection of residues of LC in real examples. And the excellent performance of this sensor will facilitate future development of rapid and high-efficiency detection of LC.

1. Introduction

Pyrethroids are known as a class of effective and popular insecticides for pest control in agriculture. In recent years, the use of pyrethroids is increasing in place of highly toxic insecticides such as organochlorines and organophosphorus insecticides [1]. However, they have been confirmed to cause developmental neurotoxicity and potential endocrine disruption effects in human beings [2,3]. Presently, more and more countries are concerned about its continues use, and the residues of pyrethroids in grain, fruit, vegetables, and animal-derived foods are strictly limited. Therefore, it is of great importance to monitor the pyrethroids residual concentration in agriculture products, which are closely related to our daily life.

Analytical methods with high sensitivity and selectivity for the detection of pesticide residues in environmental and food samples have been long-cherished for their practical monitoring purposes. To date, molecular imprinting technique, a fruitful approach to the construction of artificial receptors with tailor-made molecular recognition binding sites, has been increasingly applied to pyrethroids detection [4]. The molecularly imprinted polymers (MIPs) can be easily fabricated by the formation of non-covalent interactions or reversible covalent bonds between template molecules and functional groups [5,6]. The removal of the template from the polymerized matrix generates the binding sites that are compatible to the template. The MIPs possess several advantages over their biological counterparts, including low-cost, simple, and convenient preparation, storage stability, repeated operations without the loss of activity, high mechanical strength, durability to heat and pressure, and applicability in harsh chemical media [7–9]. Nowadays, core–shell structural MIPs have enjoyed widespread attention [10,11]. Imprinting of the outer shell layer ensures that the template sites are only situated close to the surface of the beads which allows for the rapid diffusion of ligands to and from imprinting sites. However, as we know, template molecules rebound to the recognizing sites stained in the MIPs must be removed from the MIPs and then detected via expensive and complicated instruments such as high performance liquid chromatography (HPLC) [12], gas chromatography (GC) [13], coupled column liquid chromatography with mass spectrophotometry (LC/MS) [14,15], and so forth. As we know, these methods are time-consuming and require extensive sample treatment

* Corresponding authors. Tel.: +86 511 88790683; fax: +86 511 88791800.
E-mail addresses: lcbszl@163.com (C. Liu), pjm013236@yahoo.cn (J. Pan).

http://dx.doi.org/10.1016/j.talanta.2014.02.062
0039-9140

procedures such as pressurized liquid extraction and solid-phase extraction. Additionally, removing the templates from the MIPs calls for plenty of organic solvents, thus, causing more environmental burden. Hence, the challenge is to develop an effective method for fast and high-efficiency detection of trace pyrethroids in daily-consumed foods and drinking water.

In recent years, MIPs-based fluorescence sensor, have been proposed based on surface molecularly imprinted polymers and fluorescence signal, can be applied to specifically recognize and directly quantify target analytes, independent of extracting the templates from the MIPs network and further time-consuming and complicated analysis. Li and co-workers [16] presented a general protocol for the making of surface molecular imprinting onto fluorescein-coated magnetic nanoparticles for recognition and separation of endocrine disrupting chemicals without the need for any inducers and derivatization. Zhang et al. [17] prepared the MIPs-coated CdTe composites integrating the advantages of the high selectivity of the molecular imprinting and strong fluorescence property of the QDs, which was proved to be a simple and selective sensing system for protein recognition. Combining high selectivity of MIPs and excellent fluorescent characters, these materials, with specific recognition cavity and responding to binding event with significant fluorescence intensity change, has been proven to be a good choice for convenient and high-efficiency detection of trace target analytes. To be best of our knowledge, most of the studies focus on organic dyes or QDs as the fluorescence signal, and there is few reports about lanthanide-doped phosphors tested as optosensing systems for the efficient recognition and detection of target analytes in real samples. Compared with conventional organic dyes and QDs, lanthanide-doped phosphors have the merits of high chemical stability, relatively high quantum yield, low toxicity and narrow emission spectra, and their optical properties can be flexibly tuned by variation of the lanthanide dopants and the host matrix [18,19]. The unique optical properties of lanthanide-doped phosphors have enabled them to be extensively used for fluorescent markers in cellular labeling [20], tissue imaging [21–23], fluoro-immunoassay and as donors for fluorescence resonance energy transfer [24,25].

The objective of this work is to develop a new kind of fluorescent affinity material combining the merits of molecular technology and fluorescent property of YVO_4:Eu^{3+} for specific recognition of target pyrethroids. First of all, the highly luminescent lanthanide-doped phosphors YVO_4:Eu^{3+} nanocrystals were synthesized via a simple and economical wet-chemical precipitation reactions at ambient pressure and low temperature. Then the YVO_4:Eu^{3+}, as the core substrate and fluorescence signal, was endowed with reactive vinyl groups through modification with 3-(methacryloyloxy) propyl trimethoxysilane (KH570). YVO_4:Eu^{3+}-KH570 were then further coated with a thin MIPs layer by precipitation polymerization. This imprinting layer was obtained using λ-Cyhalothrin (LC) as the model template (one of pyrethroids, on the account of its widespread use), methacrylic acid (MAA) as the functional monomer, 2,2'-azobisisobutyronitrile (AIBN) as the initiator and ethyl glycol dimethacrylate (EGDMA) as the cross-linker. The characterization, evaluation of optical stability, effect of pH, selective and sensitive determination of LC were investigated. Furthermore, we proposed a possible mechanism of the fluorescence quenching of YVO_4:Eu^{3+}@MIPs in the presence of LC. And finally, the proposed fluorescent artificial receptor (YVO_4:Eu^{3+}@MIPs) was demonstrated as a simple, rapid and selective sensing system for separating and detecting LC in real samples.

2. Experimental section

2.1. Materials

λ-Cyhalothrin (LC), β-Cyfluthrin (BC), fenvalerate (FE) and bifenthrin (BI) were purchased from Yingtianyi standard sample company (Beijing, China). Y_2O_3 (99.99%), Eu_2O_3 (99.99%) and NH_4VO_3 (99%) were purchased from Science and Technology Parent Company of the Changchun Institute of Applied Chemistry. 3-(methacryloyloxy)propyl trimethoxysilane (KH570), methacrylic acid (MAA), ethylene glycol dimethacrylate (EGDMA) and 2,2'-azobis (2-methylpropionitrile) (AIBN) were obtained from Aladdin-reagent. Doubly distilled water was used for preparing all aqueous solutions and cleaning processes. The chemical structures of monomers, template, and related compounds can be seen in Fig. 1.

2.2. Synthesis of YVO_4:Eu^{3+} Nanocrystals

In the preparation procedure, 2.0 mmol of NH_4VO_3 was added to 40 mL of deionized water and the obtained mixture was stirred vigorously for 10 min. 2.0 M NaOH solution was then introduced

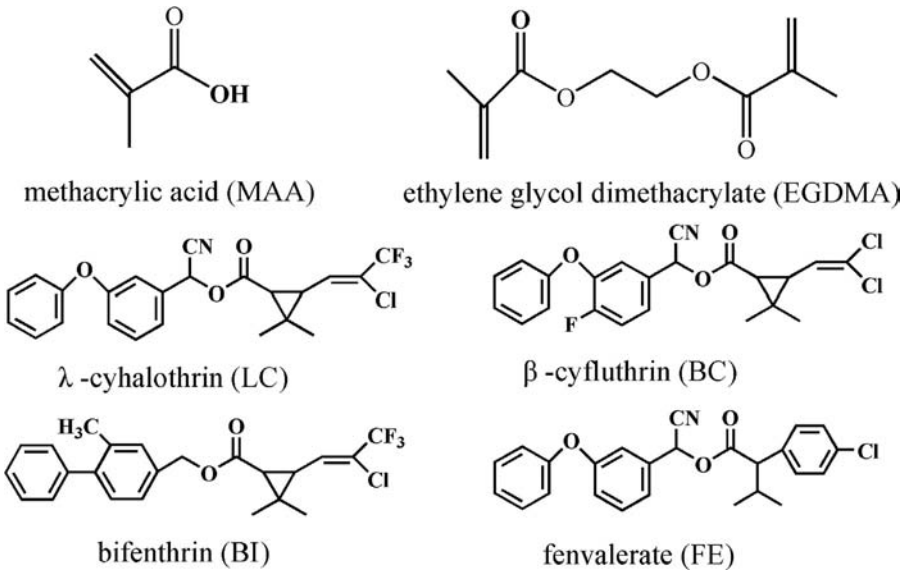

Fig. 1. Chemical structure of monomers, template and its structure analogous compounds.

into the stirred solution until pH=13 to form a clear solution. Next, 0.95 mmol Y_2O_3 and 0.05 mmol Eu_2O_3 were dissolved in dilute HNO_3, and the residual HNO_3 was removed by heating and evaporation to give clear stock solutions. Subsequently, the solution of $Y(NO_3)_3$ and $Eu(NO_3)_3$ in 40 mL of deionized water was added into the above colloidal solution dropwise. The resultant mixture was heated to 80 °C for 2 h with vigorous stirring. The final products were washed by deionized water and ethanol several times respectively and dried at 60 °C in air.

2.3. Synthesis of molecularly imprinted polymers based on YVO_4:Eu^{3+} by precipitation polymerization (YVO_4:Eu^{3+}@MIPs)

Firstly, the surface of YVO_4:Eu^{3+} was endowed with reactive vinyl groups through modification with KH570. Briefly, 0.5 g of YVO_4:Eu^{3+} nanocrystals and 5.0 mL of KH570 were dispersed into 50 mL dry toluene and stirred under nitrogen atmosphere at 80 °C for 12 h. The KH570-modified YVO_4:Eu^{3+} (YVO_4:Eu^{3+}-KH570) were then collected and washed with toluene for several times, and dried under vacuum at room temperature.

In the next step, for the coating of the LC-imprinted layer onto YVO_4:Eu^{3+}-KH570, LC (0.1 mmol) and MAA (0.4 mmol) were dispersed in the solution methanol/H_2O (4/1, v/v) (50 mL). This solution was sparged with nitrogen gas and then stored in the dark for 12 h, allowing self assembly of the LC and MAA. Next, EGDMA (2.0 mmol) and YVO_4:Eu^{3+}-KH570 (50 mg) were added into the above solution under stirring (600 rpm), to obtain the pre-polymerization solution. After purging oxygen with nitrogen gas, 10 mg of AIBN was added to the three-necked fiask while the temperature was increased to 50 °C for 6.0 h, followed by 60 °C for 18 h under nitrogen protection. The resulting products (YVO_4:Eu^{3+}@MIPs) were collected and washed thoroughly with methanol and water to remove the unreacted monomers.

The template molecules were removed by extensive washing with a mixture of methanol/acetic acid (95/5, v/v) using soxhlet extraction, until no LC leakage was observed from the YVO_4:Eu^{3+}@MIPs. Finally, the obtained YVO_4:Eu^{3+}@MIPs were dried at 50 °C under vacuum. In comparison, non-imprinted polymers (YVO_4:Eu^{3+}@NIPs) were also prepared as a blank in parallel but without the addition of LC. With the parallel evaluation of the properties of MIPs and NIPs, one can acquire information about the efficiency of imprinting. Beside the above-mentioned optimal polymerization recipe, the detailed composition of the studied polymers (P_1-P_6) are summarized in Table 1.

2.4. Determination of LC by fluorescence measurement

The fluorescence spectra analysis of the samples were carried out by dispersing 5.0 mg of YVO_4:Eu^{3+}@MIPs in 5.0 ml LC solutions with concentrations ranging from 0 to 100.0 μmol L^{-1} were added. The samples were mixed end over end at room temperature for 55 min, and measured with a Cary Eclipase fluorescence spectrometer under a 302 nm excitation light source with slit width of 5.0 nm. In this work, where F and F_0 are the fluorescence (FL) intensities of YVO_4:Eu^{3+}@MIPs at a given related concentration of LC and in a LC-free solution, respectively.

Table 1
Chemical composition of the studied MIPs and NIPs.

Polymers	YVO_4:Eu^{3+} (mg)	template (mmol)	MAA (mmol)	EGDMA (mmol)	AIBN (mg)
P_1	10.0	0.10	0.40	2.0	10.0
P_2	30.0	0.10	0.40	2.0	10.0
P_3	50.0	0.10	0.40	2.0	10.0
P_4	80.0	0.10	0.40	2.0	10.0
P_5	50.0	0.10	0.40	1.0	10.0
P_6	50.0	0.10	0.40	0.5	10.0

2.5. Sample treatment

QuEChERS (Quick, Easy, Cheap, Effective, Rugged, and Safe) has been used for sample preparation methods to help monitor residual pesticides in fruits, vegetables, and other foods [26–28]. The 10.0 g of milled blank chrysanthemum sample was extracted with 25.0 mL toluene and ethanol (50/50, v/v) in a Falcon tube. Extraction was continued with mixing, shaking for 1.0 min, adding 0.5 g NaCl, and then centrifuging at 4000 rpm at −5 °C for 5.0 min. The supernatant was transferred to a 15 mL Falcon tube containing 0.75 g $MgSO_4$. After shaking for 90 s and centrifuging for 5.0 min at 4000 rpm at −5 °C, 4.0 mL of supernatant was transferred to a 5.0 mL vial and evaporated to dryness under a gentle stream of nitrogen gas. The residue was dissolved in methanol/H_2O (4/1, v/v) to obtain 5.0 mL solution, and after dispersing 5.0 mg of YVO_4:Eu^{3+}@MIPs end over end at room temperature for 55 min, fluorescence spectra analysis was carried out.

2.6. Recovery determination

The blank chrysanthemum and water samples spiked at concentrations of 5.0, 10.0, and 20.0 μmol L^{-1} were prepared in triplicate, correspondingly. And then treated according to the procedure described in sample preparation section. The recoveries for each pesticide were calculated using calibration standards based on the Stern–Volmer-type plots and ultraviolet spectra as a reference method.

2.7. Characterization

The X-ray diffraction (XRD) patterns of the samples were carried out on a D8 ADVANCE diffractometer (Bruker) with use of Cu-Ka radiation. Infrared spectra (4000−400 cm^{-1}) were collected on a Nicolet NEXUS-470 FT-IR apparatus (USA) using KBr disks. Scanning electron microscopy (SEM) images were recorded by JSM-7001-F. Transmission electron microscopy (TEM) images were recorded by a JEM-2100 (HR) electron microscope. Fluorescence spectra was taken on a Cary Eclipase fluorescence spectrometer (USA).

3. Results and discussion

3.1. Preparation of the molecularly imprinted polymers

We put here forward a simple and sensitive method for determination of pyrethroids based on MIPs-based fluorescence sensor. First of all, the highly luminescent YVO_4:Eu^{3+} nanocrystals were synthesized via a simple and economical wet-chemical precipitation reactions at ambient pressure and low temperature. Then precipitation polymerization was chosen as a straightforward and beneficial route to coat YVO_4:Eu^{3+} with a thin MIPs layer for the synthesis of core–shell structured nanoparticles, and the synthesis route was shown in Scheme 1a. In this study, a mixture of methanol and water (4/1, v/v) was chosen as polymerization medium instead of the poisonous solvent such as acetonitrile or toluene [29]. In addition, MAA was chosen as an established functional comonomer responsible for the creation of selective recognition sites by interaction with the LC molecules through multipoint H-bonding [30], and the mole ratio of LC/MAA=4/1 was determined by UV spectroscopic analysis (Supporting information, Fig. S1). The required relative amounts of EGDMA and

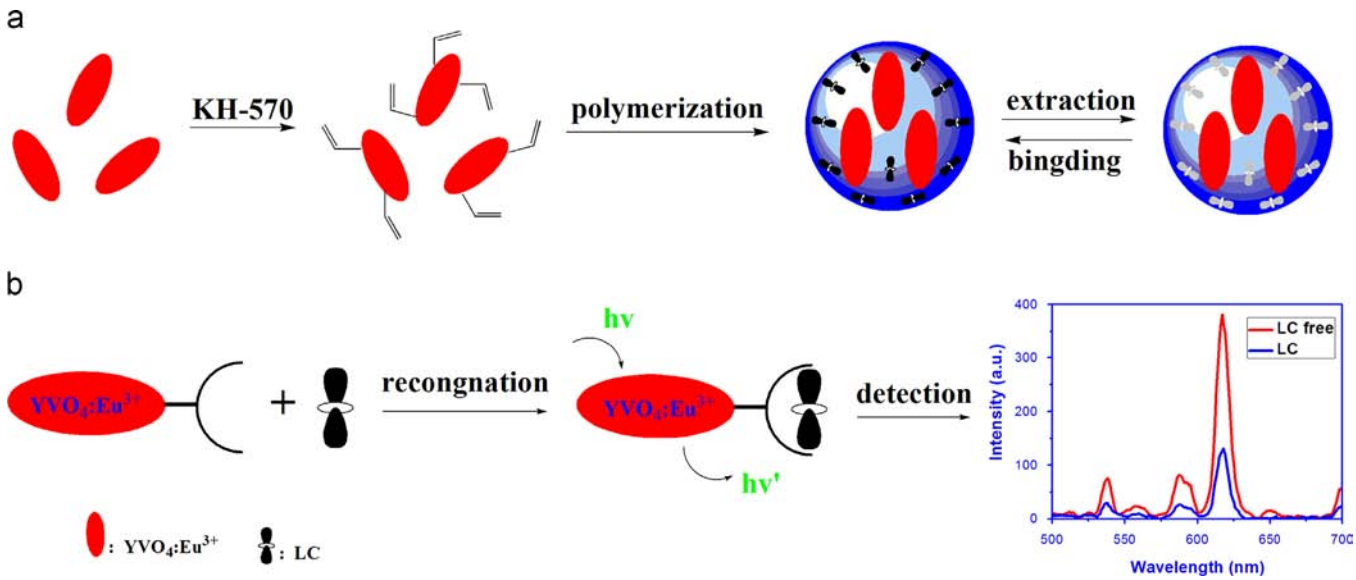

Scheme 1. Schematic illustration of the fabrication of $YVO_4:Eu^{3+}$@MIPs (a) and its possible quenching mechanism for the detection of LC (b).

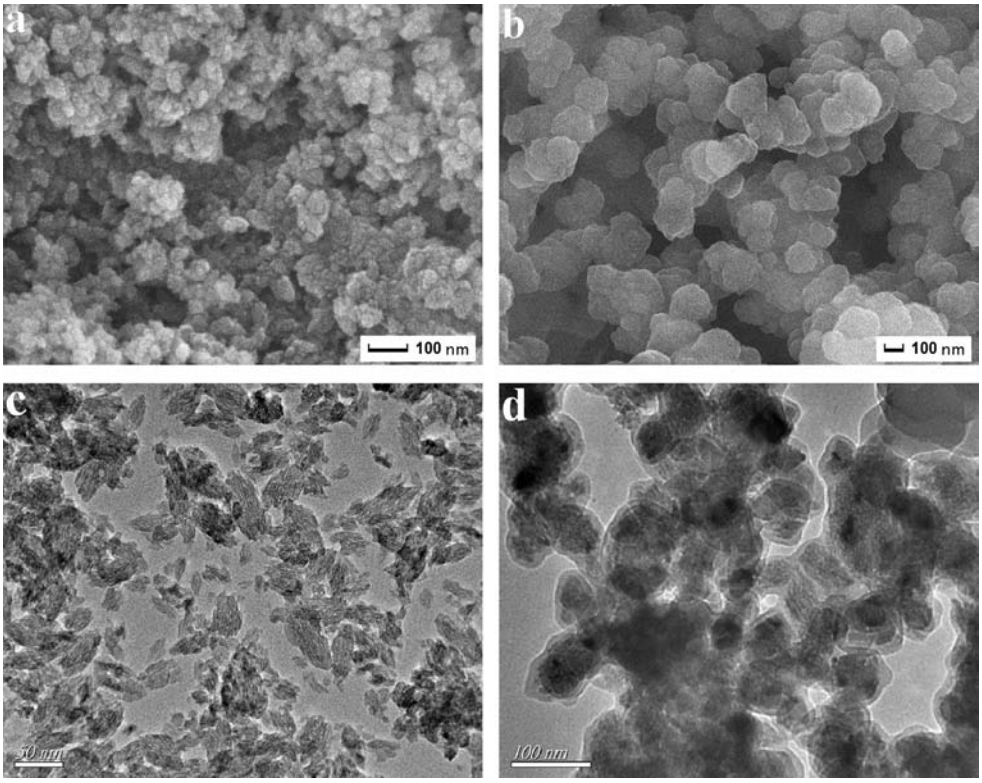

Fig. 2. SEM and TEM images of $YVO_4:Eu^{3+}$ (a and c) and $YVO_4:Eu^{3+}$@MIPs (b and d).

MAA as well as the quantity of the $YVO_4:Eu^{3+}$ nanocrystals were explored by preparing polymers with different composition. In all these studies, the dosage of template was 0.10 mmol. TEM images were recorded to evaluated the property of the imprinted polymers. The TEM images for different imprinted polymers (P_1-P_6) were shown in supporting information (Figs. S2 and S3). And the optimized core–shell structured imprinted polymers P_3 were obtained when 0.4 g polymerization precursors and 50 mg $YVO_4:Eu^{3+}$ nanocrystals were used, as could be seen in Fig. 2b and d.

3.2. Morphological characterization

The morphology of $YVO_4:Eu^{3+}$ nanocrystals and the polymer nanoparticles with the optimal composition (P_3) were investigated by SEM and TEM, see Fig. 2. Fig. 2a and c showed representative images of the prepared $YVO_4:Eu^{3+}$, which were spindle-like nanoparticles with equatorial diameters of 30–50 nm and lengths of 80–120 nm. Using such $YVO_4:Eu^{3+}$ nanoparticles as seeds, fluorescence polymer spheres with high fluorescence intensity

and a well-defined core–shell structure was obtained by encapsulating nanoparticles within a thin polymer matrix. Fig. 2d revealed that the prepared core–shell structured fluorescence MIPs had shell thicknesses of about 7–25 nm, whereas the SEM image (Fig. 2b) proved that these core–shell particles had an even surface morphology, which endowed them with both the special surface property and the large external surface area that was desirable for molecular immobilization. In addition, the corresponding EDS spectrum in Fig. S4 (Supporting information) also confirmed the existence of YVO_4:Eu^{3+} in the core–shell structured fluorescence polymer spheres.

3.3. X-ray diffraction (XRD)

The formation of YVO_4:Eu^{3+} could be confirmed by wide angle X-ray diffraction characterization. Fig. 3 showed the XRD patterns of the as-formed YVO_4:Eu^{3+}@MIPs (red) and YVO_4:Eu^{3+}@NIPs (blue) composite and pure YVO_4:Eu^{3+} (black). The three peaks at 2θ= 24.88°, 2θ= 33.55° and 2θ= 49.77° could be indexed to the (200), (112) and (312) reflections of YVO_4, suggesting that the successful crystallization of YVO_4:Eu^{3+} has formed based on the wet-chemical method [31]. Compared with YVO_4:Eu^{3+}, the peaks intensity of YVO_4:Eu^{3+}@MIPs and YVO_4:Eu^{3+}@NIPs decreased in some extent, which could attributed to the layer imprinted polymers coated at the the surface of YVO_4:Eu^{3+}.

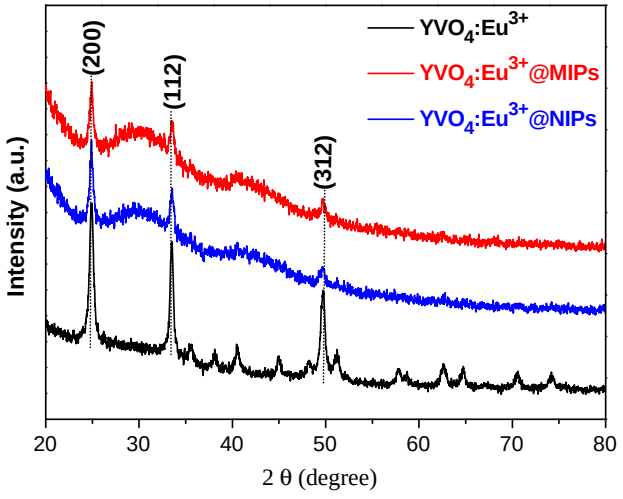

Fig. 3. X-ray diffraction patterns of YVO_4:Eu^{3+} (black), YVO_4:Eu^{3+}@MIPs (red) and YVO_4:Eu^{3+}@NIPs (blue). (For interpretation of the references to color in this figure legend, the reader is referred to the web version of this article.)

3.4. Fluorescence spectroscopic characterization

As shown in Fig. 4a, the YVO_4:Eu^{3+}@MIPs in water exhibited strong red luminescence under UV excitation with a wavelength of 254 nm. Fig. 4b showed photoluminescence excitation, emission of YVO_4:Eu^{3+}, YVO_4:Eu^{3+}@NIPs, and YVO_4:Eu^{3+}@MIPs spectra. The doping concentration of Eu^{3+} was 5.0 mol% of Y^{3+} in YVO_4,which had been previously optimized for photoluminescence intensity [32,33]. The excitation spectrum consisted of an intense band centered at 302 nm monitored at 617 nm (the Eu^{3+} emission of $5D^0$–$7F^2$). Compared with the FL intensity of YVO_4:Eu^{3+}, the intensity of YVO_4:Eu^{3+}@NIPs and YVO_4:Eu^{3+}@MIPs decreased to some extent, which was a result of the polymer layers that coated at the surface of YVO_4:Eu^{3+}.

3.5. Infrared spectroscopic characterization

The FT-IR spectra of YVO_4:Eu^{3+}, YVO_4:Eu^{3+}-KH570, YVO_4:Eu^{3+}@MIPs and YVO_4:Eu^{3+}@NIPs were shown in Fig. 5. In Fig. 5, for the the pure YVO_4:Eu^{3+} nanocrystals (a), a strong absorption peak at 826 cm^{-1} and a weak one at 454 cm^{-1} appeared, which were attributed to the absorption of V–O (from VO_4^{3-} group) and Y (Eu)–O bonds, respectively [34,35]. This suggested that crystalline phase (YVO_4) has formed, agreeing well with the results of XRD. After the modification of KH570, as it shown in Fig. 5(b), the characteristic absorption of YVO_4:Eu^{3+} nanocrystals have weakened, there came out two new absorption at 1637 cm^{-1} and 1716 cm^{-1}, which might attribute to C=C stretching mode and C=O stretching vibration of KH570, respectively. This indicated that the surface of the YVO_4:Eu^{3+} was successfully endowed with reactive vinyl groups through modification with KH570. Furthermore, the FT-IR of YVO_4:Eu^{3+}@MIPs (c) and YVO_4:Eu^{3+}@NIPs (d) possessed of the same absorption bands around 1730, 1253, and 1157 cm^{-1}, which were assigned to C=O stretching vibration of carboxyl (MAA), C−O asymmetric and symmetric stretching vibration of ester (EGDMA), respectively [36]. The medium peaks

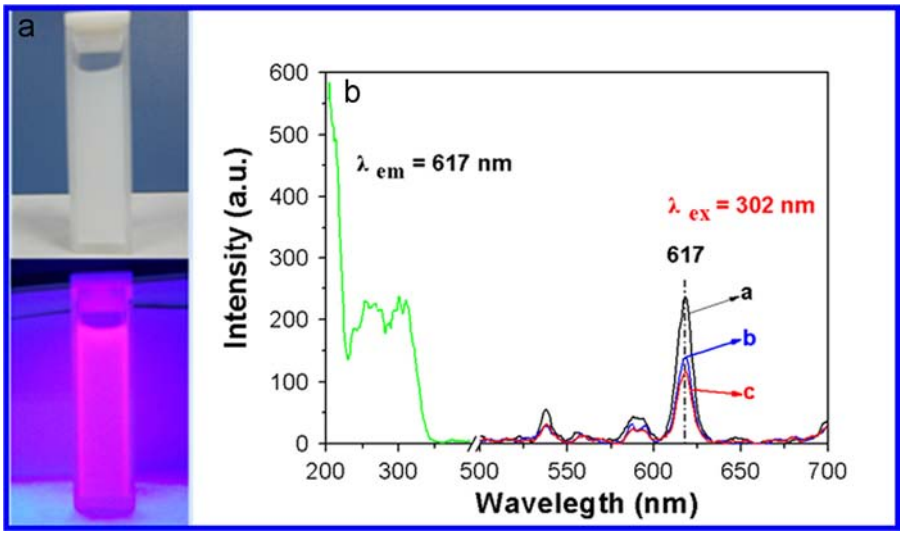

Fig. 4. (a) Digital photographs of YVO_4:Eu^{3+}@MIPs dispersed in water under daylight (up) and 254 nm UV light (down) irradiation. (b) Photoluminescence excitation (green), emission of YVO_4:Eu^{3+} (a) and YVO_4:Eu^{3+}@NIPs (b) and YVO_4:Eu^{3+}@MIPs (c). (For interpretation of the references to color in this figure legend, the reader is referred to the web version of this article.)

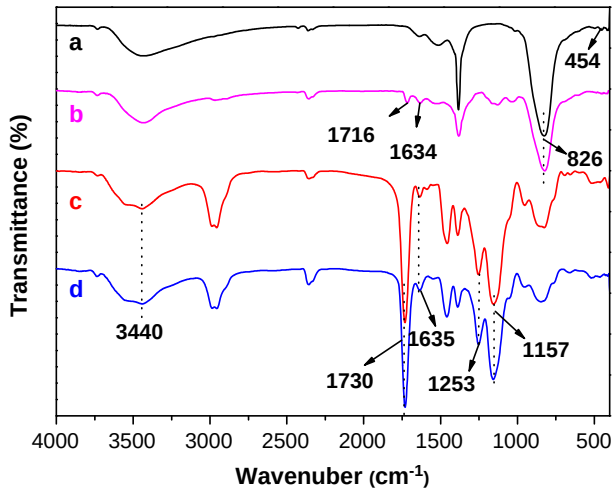

Fig. 5. FT-IR spectra of YVO_4:Eu^{3+} (a), YVO_4:Eu^{3+}-KH570 (b), YVO_4:Eu^{3+}@MIPs (c) and YVO_4:Eu^{3+}@NIPs (d).

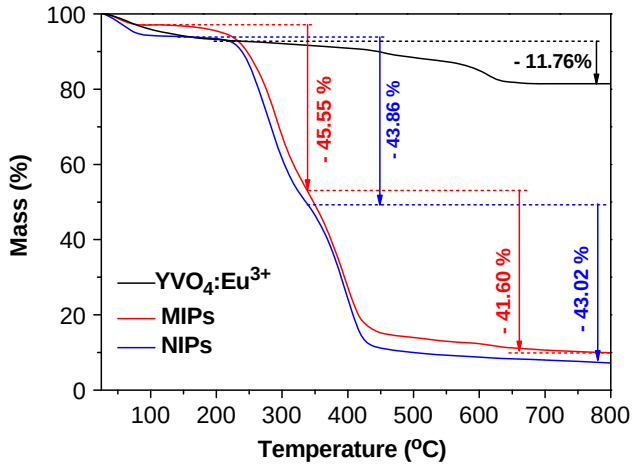

Fig. 6. Thermogravimetric analysis curves of YVO_4:Eu^{3+} (black), YVO_4:Eu^{3+}@MIPs (red) and YVO_4:Eu^{3+}@NIPs (blue). (For interpretation of the references to color in this figure legend, the reader is referred to the web version of this article.)

at 1635 cm^{-1}, which corresponded to the C=C stretching mode of methacrylic vinyl groups, suggested that less than 100% of bonded EGDMA molecules were cross-linked in the polymers. Meanwhile, the absorption band at 3440 cm^{-1} of the polymers could be attributed to the stretching vibration of O–H bonds from MAA molecules. All the results confirmed that the cross-linking reaction was successfully initiated in the presence of AIBN.

3.6. Thermogravimetric analysis (TGA)

The degree of polymerization for YVO_4:Eu^{3+}@MIPs and YVO_4:Eu^{3+}@NIPs were evaluated by TGA under N_2 atmosphere. As shown in Fig. 6, there were three weight loss stages: the first weight loss stage could be ascribed to the evaporation of water molecules for each particle, which were 2.95%, 5.84% for YVO_4:Eu^{3+}@MIPs and YVO_4:Eu^{3+}@NIPs, respectively. The second weight loss stage started from 100 °C to 340 °C and the last stage was from 340 °C to 800 °C. In the last two stages (from 100 °C to 800 °C), there were no significant differences of the mass loss of the YVO_4:Eu^{3+}@MIPs and YVO_4:Eu^{3+}@NIPs, which were 87.15% and 86.88% for YVO_4:Eu^{3+}@MIPs and YVO_4:Eu^{3+}@NIPs, respectively. Compared with YVO_4:Eu^{3+}@MIPs and YVO_4:Eu^{3+}@NIPs, YVO_4:Eu^{3+} cannot be easily decomposed at high temperatures, which showed little weight loss (11.76% below 800 °C). Thus, the remaining mass for the YVO_4:Eu^{3+}@MIPs and YVO_4:Eu^{3+}@NIPs were attributed to the thermal resistance of YVO_4:Eu^{3+} particles, and the quantity of YVO_4:Eu^{3+} particles in the YVO_4:Eu^{3+}@MIPs and YVO_4:Eu^{3+}@NIPs were 9.90% and 7.28%, respectively.

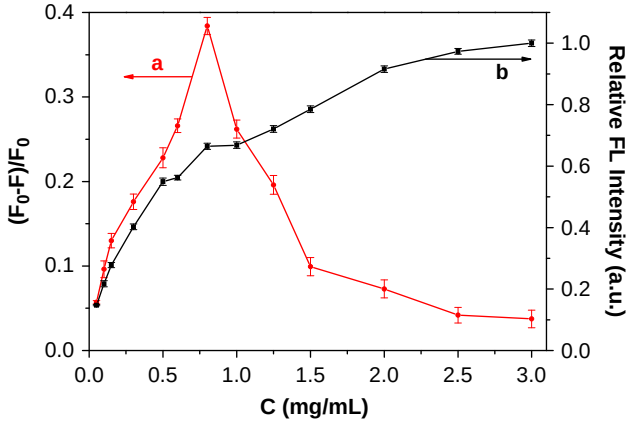

Fig. 7. Effects of the concentration of YVO_4:Eu^{3+}@MIPs on FL intensity. Curve a: the function of variation rate of FL intensity of detection system (containing YVO_4:Eu^{3+}@MIPs + 50.0 μmol L^{-1} LC) vs. concentration of YVO_4:Eu^{3+}@MIPs; curve b: the function of relative FL intensity vs. concentration of YVO_4:Eu^{3+}@MIPs.

3.7. Optimization of the experimental conditions

To achieve an optimal analytical performance of the developed MIPs-based fluorescence sensor, the concentration of YVO_4:Eu^{3+}@MIPs, the pH and the detection time should be optimized.

3.8. Concentration of YVO_4:Eu^{3+}@MIPs

The concentration of YVO_4:Eu^{3+}@MIPs from 0.05 mg mL^{-1} to 3.0 mg mL^{-1} was used to study the effects on the LC detection system. As for the analysis principle of this detection system was based on the FL quenching of YVO_4:Eu^{3+}@MIPs, both detection sensitivity and linear range into consideration were important for the detection system. Maintaining YVO_4:Eu^{3+}@MIPs of high FL intensity could obtain wide linear range; meanwhile, the variation rate of FL intensity $[(F_0-F)/F_0]$ (F_0 and F represent for the FL intensity before and after adding LC into the system) determined the analysis sensitivity. As shown in Fig. 7, when the concentration of YVO_4:Eu^{3+}@MIPs was low, a small amount of LC could result in great degree of the FL quenching, and high sensitivity (curve a) could be achieved but with a narrow linear range (curve b); when the YVO_4:Eu^{3+}@MIPs was in higher levels, FL intensity of system was increased, while the FL quenching degree was relatively small. As a result, a concentration of 1.0 mg mL^{-1} was chosen for the detection of LC [37].

3.9. Effect of pH

The effect of pH on the FL intensity in a range between 2.0 and 12 was studied for YVO_4:Eu^{3+} and YVO_4:Eu^{3+}@MIPs in Fig. 8a. At the beginning of 12 h, the FL intensity of YVO_4:Eu^{3+} at 2.0 and 12 was enhanced. As time went on, the FL intensity at 2.0 and 12 decreased gradually, while at pH=7.0, the FL intensity was considerably stable. This was probably because the crystallite structure of YVO_4:Eu^{3+} was damaged in strong acidic and alkaline media, which weaken the energy transfer from VO_4^{3-} to Eu^{3+} ions [38]. As for YVO_4:Eu^{3+}@MIPs, the results proved that pH had almost no effect on the FL intensity, which was on account of the protecting imprinted polymers that coated at the surface of YVO_4:Eu^{3+}. Further studying the effect on the variation rate of FL

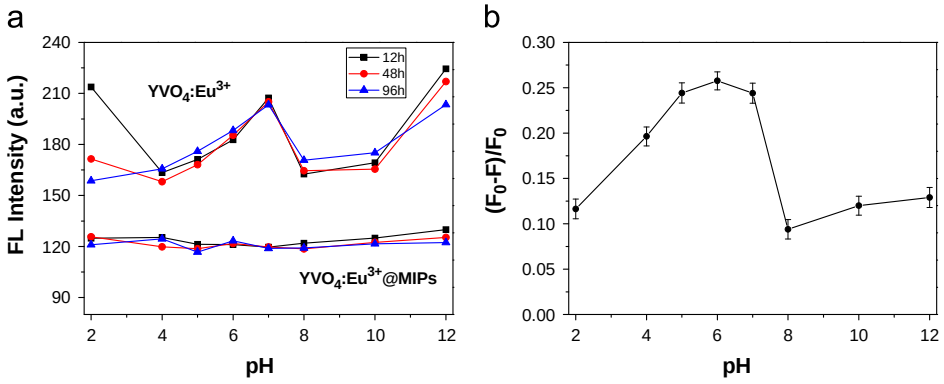

Fig. 8. Effects of different pH on the FL intensity of $YVO_4:Eu^{3+}$ and $YVO_4:Eu^{3+}$@MIPs (a) and the variation rate of FL intensity response toward LC. (b) (Experiment condition: $YVO_4:Eu^{3+}$@MIPs, 1.0 mg mL^{-1}; LC, 50.0 μmol L^{-1}).

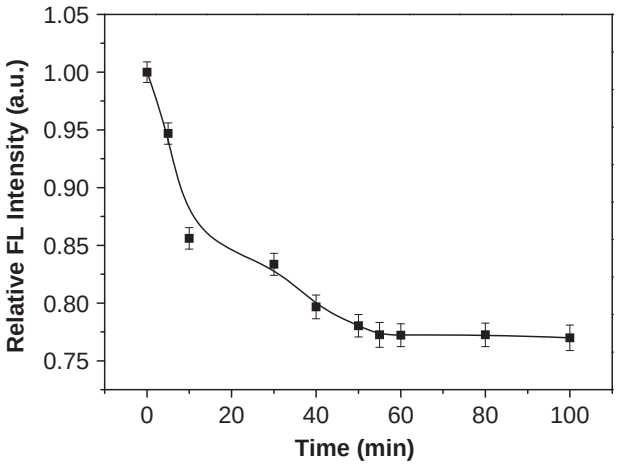

Fig. 9. Effect of time on FL intensity. (Experiment condition: $YVO_4:Eu^{3+}$@MIPs, 1.0 mg mL^{-1}; LC, 50.0 μmol L^{-1}).

intensity response toward LC (the concentration of LC was 50 μmol L^{-1}), as was shown in Fig. 8b, we found that the the variation rate of FL intensity $[(F_0-F)/F_0]$ increased over the pH range of 2.0–6.0 and then declined in the pH range of 6.0–12. It is probably because the pKa of MAA is about 5.80 [39], when the pH > pKa values, MAA got deprotonated and then hydrogen bonds were disrupted between MAA and LC. As a result, a pH of 6.0 was selected for the further experiments.

3.10. Detection time

To determine the optimal detection time, a certain amount of LC (50 μmol L^{-1}) was mixed with $YVO_4:Eu^{3+}$@MIPs (1.0 mg mL^{-1}), and the FL intensities were recorded at different interval time. As shown in Fig. 9, the FL intensity decreased at the initial beginning, when time was up to 55 min, the FL intensity was almost the same. As a result, we chose 55 min for the optimal detection time.

3.11. Determination of pyrethroids

Under the optimal conditions, the developed MIPs-based fluorescence sensor was employed for quantifying LC standards with various concentrations based on FL quenching of $YVO_4:Eu^{3+}$@MIPs. The assay was carried out in methanol and H_2O mixture after incubation target LC with $YVO_4:Eu^{3+}$@MIPs for 55 min at room temperature, and the $YVO_4:Eu^{3+}$@NIPs were used for comparison. As shown in Fig. 10a, the FL intensity of the $YVO_4:Eu^{3+}$@MIPs turned out to be decreased sensitively in the presence of a certain amount of LC. The relationship between the FL intensity and the concentration of quenching LC could be described by the Stern–Volmer equation [40,41]

$$F_0/F = 1 + K_{SV}[c]$$

where F and F_0 are the FL intensities of $YVO_4:Eu^{3+}$@MIPs at a given related concentration of LC and in a LC-free solution, respectively. K_{sv} is the Stern–Volmer quenching constant, and [c] is the concentration of LC. Showed in Fig. 10b, we found that two linear dependences between F_0/F and the concentration of LC were obtained, which was a little different from the previous reports [16,42]. Except for the linear dependence ($F_0/F = 1.220 + 0.00226c$) at the range from 10.0–90.0 μmol L^{-1} with a correlation coefficient of 0.9930, another linear dependence ($F_0/F = 1.145 + 0.0107c$) at the lower concentration (2.0–10.0 μmol L^{-1}) was achieved with a correlation coefficient of 0.9864. We speculated that the initial quench stage might be priority to nonspecific bindings between the template LC and $YVO_4:Eu^{3+}$@MIPs, and the second stage could attribute to the specific bindings because of the presence of selective binding sites in the obtained $YVO_4:Eu^{3+}$@MIPs. More inspiringly, the developed MIPs-based fluorescence sensor did not require much sample separation and a complicated wash procedure for the LC detection.

3.12. Selectivity and sensitivity determination

To obtain the binding affinity properties of specific imprinted binding sites ($YVO_4:Eu^{3+}$@MIPs) and nonspecific sites ($YVO_4:Eu^{3+}$@NIPs), the FL analysis has been carried out. The quench amount between the FL intensities of the imprinted receptor ($YVO_4:Eu^{3+}$@MIPs and $YVO_4:Eu^{3+}$@NIPs) at a given related pyrethroids (LC and FE) concentration and in a pyrethroids free solution was taken as equal as the uptake amounts. According to the obtained results (Fig. 10a), the quench amount of binding LC by $YVO_4:Eu^{3+}$@MIPs increased significantly with the concentrations of LC in solution (■). However, the $YVO_4:Eu^{3+}$@NIPs did not exhibit the obvious difference in the quench amount of rebinding capacities of LC (●) and FE (▾), which indicated the $YVO_4:Eu^{3+}$@MIPs have a better selectivity and sensitivity than those of $YVO_4:Eu^{3+}$@NIPs. Therefore, the FL analysis was more suitable for the on-site and rapidly detect analysis. Further, the selectivity of the developed MIPs-based fluorescence sensor was also investigated by spiking LC, BC, BI and FE in the incubation solution, respectively. As evident from Fig. 11, the quench amount of $YVO_4:Eu^{3+}$@MIPs for the four compounds followed the order LC > BC > BI > FE. By calculation, the differences between the quench amount of $YVO_4:Eu^{3+}$@MIPs and $YVO_4:Eu^{3+}$@NIPs were 0.024, 0.0087, 0.00077, 0.0062 at 5.0 μmol L^{-1} and 0.042, 0.010, 0.0074, 0.011 at 50.0 μmol L^{-1} for LC, BC, FE, and BI, respectively.

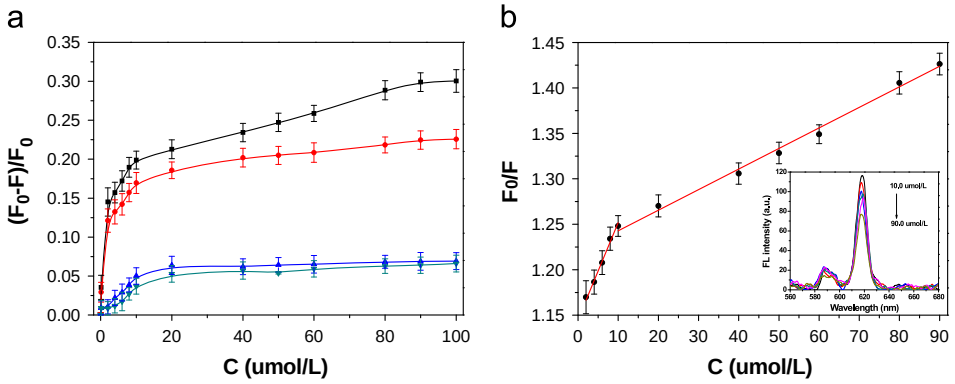

Fig. 10. (a) The quenching amount of YVO_4:Eu^{3+}@MIPs and YVO_4:Eu^{3+}@NIPs by LC (black squares and red circles) and FE (blue up-pointing triangles and dark cyan down-pointing triangles) at different concentration and (b) Stern–Volmer-type description of the data showing a linear fit throughout the LC concentration range. Inset b: fluorescence spectra of the YVO_4:Eu^{3+}@MIPs with the increasing concentrations of LC. (For interpretation of the references to color in this figure legend, the reader is referred to the web version of this article.)

Table 2
Test for the Interference of different substances on the fluorescence of YVO_4:Eu^{3+}@MIPs (experiment condition: YVO_4:Eu^{3+}@MIPs, 1.0 mg mL^{-1}; LC, 50.0 μmol L^{-1}).

Coexisting substance	Coexisting concentration (μmol L^{-1})	Change of fluorescence intensity (%)
K^+	5.0	0.48
Na^+	5.0	0.69
Ca^{2+}	2.0	1.97
Mg^{2+}	2.0	1.74
Cl^-	1.0	0.97
SO_4^{2-}	2.0	0.65
NO_3^-	2.0	1.24
CO_3^{2-}	1.0	1.15

Table 3
Recovery of LC in water sample (1) and chrysanthemum sample (2) with LC solution at different concentration levels (experiment condition: YVO_4:Eu^{3+}@MIPs, 1.0 mg mL^{-1}; n=5).

Sample	Concentration taken (μmol L^{-1})	Found (μmol L^{-1})		Recovery (%)		RSD (%)	
		FL	UV	FL	UV	FL	UV
1	5.0	4.928	4.951	98.56	99.02	2.3	1.4
	10.0	9.963	9.869	99.63	98.69	1.6	0.89
	20.0	19.961	19.874	99.81	99.37	1.2	0.74
2	5.0	4.927	4.943	98.54	98.86	2.4	1.6
	10.0	9.965	9.953	99.65	99.53	1.5	0.94
	20.0	19.972	19.964	99.86	99.82	1.4	0.76

The specific template bindings (normally defined as the quench amount difference between the MIPs and its corresponding NIPs [43]) at 50.0 μmol L^{-1} were somewhat higher than that at lower concentration (5.0 μmol L^{-1}), which could effectively support the results as it shown in Fig. 10b. The results above suggested that YVO_4:Eu^{3+}@MIPs were specific to LC but nonspecific to other pesticides. Due to the distinct sizes, structures, and functional groups of the template, different binding forces could form between the pesticides and MAA, resulting in a different recognition effect [44]. Therefore, the developed MIPs-based fluorescence sensor possessed an acceptable selectivity.

To investigate the interfering effects of sample matrix components on the analytical properties of the developed MIPs-based fluorescence sensor, several possible components in the water, such as K^+, Na^+, Ca^{2+}, Mg^{2+}, Cl^-, SO_4^{2-}, NO_3^-, and CO_3^{2-}, were added into the incubation solution containing 50 μmol L^{-1} LC, respectively. As shown in Table 2, these interfering ions did not almost affect the significant change in the FL intensity to target LC alone. Therefore, YVO_4:Eu^{3+}@MIPs could be used for highly selective analysis of LC in the presence of other commonly interfering ions and pyrethroids. It was rational that the high specificity of the MIPs-based fluorescence sensor might be ascribed to the memory of specific imprinted binding sites (cavities) in YVO_4:Eu^{3+}@MIPs.

3.13. Application to sample analysis

To monitor the possible application of the developed MIPs-based fluorescence sensor for real samples, LC standards with various concentrations were spiked into two samples, such as surface river water and chrysanthemum. The as-prepared specimens were measured by using the fluorescence spectra and ultraviolet spectra as a reference method. The assay results using these two methods were listed in Table 3. Compared with the UV method, we found that the stability of the FL quenching method was less than that of the UV method, but the detect results were more accurate and sensitivity. The results revealed a good accordance between both analytical methods, thereby the developed MIPs-based fluorescence sensor could be regarded as an optional scheme for quantitative determination of LC.

3.14. Regenerability

Regenerability was a key factor for an effective detection analysis. The YVO_4:Eu^{3+}@MIPs particles were required to be regenerative for multiple cycles to reduce the cost, which was very important for industrial applications. In this study, a mixture of methanol/acetic acid (95/5, v/v) elution was adopted, the effects of the regeneration times were shown in Fig. 12. In comparison with fresh YVO_4:Eu^{3+}@MIPs, there was only a little change in the FL intensity after the detection process and it could recycle at least six times for the LC detection.

3.15. Fluorescence quenching mechanism

Generally, there are three types of FL quenching mechanisms: static quenching, dynamic quenching, and a combination of the two. For a single dynamic or static quenching process, the change in the FL intensity (F_0/F) has a linear relationship with the quenching reagent concentration (C), whereas the Stern–Volmer curve is non-linear and has an upward movement when the quenching process is a combination of the two. Moreover, for dynamic quenching, the maximum quenching constant of

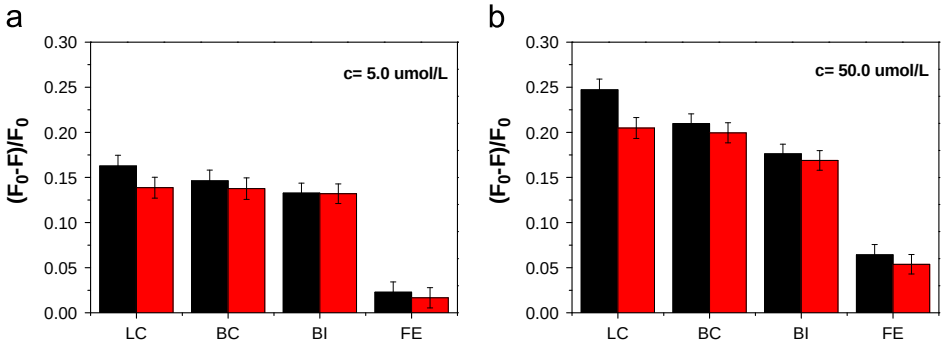

Fig. 11. The quenching amount of YVO_4:Eu^{3+}@MIPs and YVO_4:Eu^{3+}@NIPs by different kinds of pyrethroids at concentration of 5.0 μmol L^{-1} (a) and 50.0 μmol L^{-1} (b).

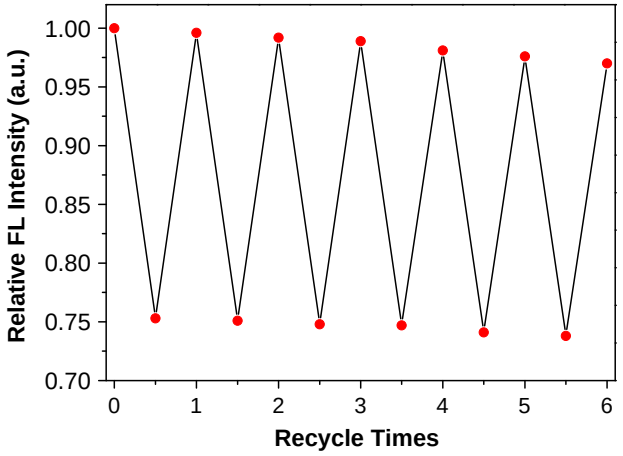

Fig. 12. Stability and potential regeneration of the YVO_4:Eu^{3+}@MIPs.

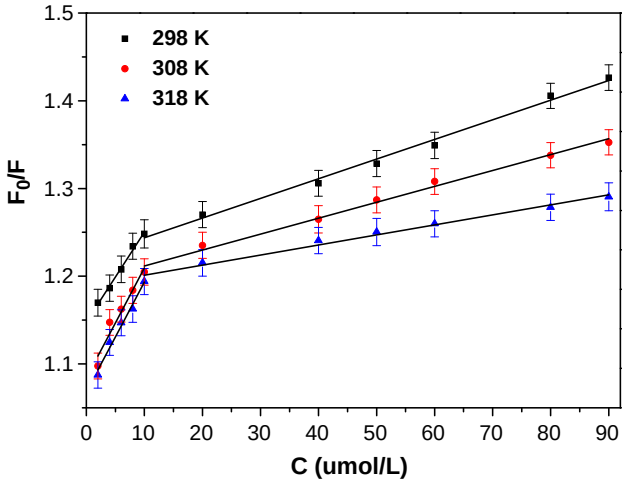

Fig. 13. Stern–Volmer-type plots of LC with YVO_4:Eu^{3+}@MIPs at different temperatures.

molecules is usually less than 100 L mol^{-1}. If the quenching constant is more than 100 L mol^{-1}, the FL quenching process is static [45]. The results of our experiments showed that the curve was linear (Fig. 10b), and the quenching constants (1.066×10^4 L mol^{-1} and 2.260×10^3 L mol^{-1}) were more than 100 L mol^{-1}. Hence, the quenching mechanism was considered to be static.

In the case of YVO_4:Eu^{3+}@MIPs, as shown in Scheme 1b, the specific binding effect between LC and the recognition site leads to the strong adsorption of LC, leading to the FL quenching behavior through their hydrogen bonding interactions at close proximity, and confirming that static quenching is a predominant process. To confirm this speculation, a systematic study of the quenching mechanism was carried out. Fig. 13 showed the comparison of Stern–Volmer plots for LC at different temperatures. A decrease in the quenching constant was observed in association with an increase in temperature, which was due to the formation of a ground-state complex between YVO_4:Eu^{3+}@MIPs and LC [46], and suggested the occurrence of static quenching [47]. Therefore, the quenching was concluded to be static in nature.

4. Conclusions

A highly sensitive, selective, and convenient method for LC analysis has been developed on the basis of the fluorescence quenching of YVO_4:Eu^{3+}@MIPs. The core–shell structured YVO_4:Eu^{3+}@MIPs were demonstrated of good pH stability and employed as a convenient and highly sensitive luminescence probe for optical recognition of LC. Quenching of the luminescence emitted by the core–shell structured nanoparticles allowed the determination of LC as low as 1.76 μM. The YVO_4:Eu^{3+}@MIPs also exhibited steady and excellent reusable performance toward LC in at least six sorption–adsorption cycles, and the fluorescence-quenching mechanism was proven to be static quenching in our study. And the developed MIPs-based fluorescence sensor was proven to be an optional scheme for quantitative determination of LC using the UV method as a reference. Furthermore, molecular recognition of YVO_4:Eu^{3+}@MIPs is in progress in our laboratory, which would spark a broad spectrum of interest because of its great versatility and flexibility for future applications.

Acknowledgments

This work was financially supported by the National Natural Science Foundation of China (Nos. 21107037, 21176107 and 21277063), National Postdoctoral Science Foundation (No. 2013M5 30240), Postdoctoral Science Foundation funded Project of Jiangsu Province (No. 1202002) and Programs of Senior Talent Foundation of Jiangsu University (No. 12JDG090) and Natural Science Foundation of Jiangsu Province (BK2012701).

Appendix A. Supporting information

Supplementary data associated with this article can be found in the online version at http://dx.doi.org/10.1016/j.talanta.2014.02.062.

References

[1] H.C. Oudou, R.M. Alonso, H.C. Bruun Hansen, Anal. Chim. Acta 523 (2004) 69–74.
[2] T.J. Shafer, D.A. Meyer, K.M. Crofton, Environ. Health Perspect. 113 (2005) 123–136.
[3] I.Y. Kim, J.H. Shin, H.S. Kim, S.J. Lee, I.H. Kang, T.S. Kim, H.J. Moon, K.S. Choi, A. Moon, S.Y. Han, J. Reprod. Dev. 50 (2004) 245–255.
[4] Y. Guo, X. Liang, Y. Wang, Y. Liu, G. Zhu, W. Gui, J. Appl. Polym. Sci. 128 (2013) 4014–4022.
[5] C. Baggiani, C. Giovannoli, L. Anfossi, C. Passini, P. Baravalle, G. Giraudi, J. Am. Chem. Soc. 134 (2012) 1513–1518.
[6] J. Mathew-Krotz, K.J. Shea, J. Am. Chem. Soc. 118 (1996) 8154–8155.
[7] C. Zheng, Y.P. Huang, Z.S. Liu, Anal. Bioanal. Chem. 405 (2013) 2147–2161.
[8] L. Chen, J. Liu, Q. Zeng, H. Wang, A. Yu, H. Zhang, L. Ding, J. Chromatogr. A 1216 (2009) 3710–3719.
[9] C.H. Lu, W.H. Zhou, B. Han, H.H. Yang, X. Chen, X.R. Wang, Anal. Chem. 79 (2007) 5457–5461.
[10] Y.X. Liu, G.Q. Jian, X.W. He, L.X. Chen, Y.K. Zhang, J. Chin, Anal. Chem. 41 (2013) 161–166.
[11] Y. Liu, Y. He, Y. Jin, Y. Huang, G. Liu, R. Zhao, J. Chromatogr. A 1323 (2014) 11–17.
[12] M. Mezcua, O. Malato, J.F. García-Reyes, A. Molina-Díaz, A.R. Fernandez-Alba, Anal. Chem. 81 (2009) 913–929.
[13] R.E. Hunter, J.R. A.M. Riederer, P.B. Ryan, J. Agric. Food Chem. 58 (2010) 1396–1402.
[14] B. Mayer-Helm, J. Chromatogr. A 1216 (2009) 8953–8959.
[15] A.P. Vonderheide, P.E. Kauffman, T.E. Hieber, J.A. Brisbin, L.J. Melnky, J. N. Morgan, J. Agric. Food Chem. 57 (2009) 2096–2104.
[16] Y. Li, C. Dong, J. Chu, J. Qi, X. Li, Nanoscale 3 (2011) 280–287.
[17] W. Zhang, X.W. He, Y. Chen, W.Y. Li, Y.K. Zhang, Biosens. Bioelectron. 26 (2011) 2553–2558.
[18] F. Wang, X.G. Liu, Chem. Soc. Rev. 38 (2009) 976–989.
[19] W.J. Zhang, Q. Jiang, X.Y. Wang, G. Song, X.X. Shao, Z.Y. Guo, J. Pept. Sci. 19 (2013) 350–354.
[20] C.R. Patra, R. Bhattacharya, S. Patra, S. Basu, P. Mukherjee, D. Mukhopadhyay, J. Nanobiotechnol. 4 (2006) 11–25.
[21] J. Zhou, M. Yu, Y. Sun, X. Zhang, X. Zhu, Z. Wu, D. Wu, F. Li, Biomaterials 32 (2011) 1148–1156.
[22] L.Q. Xiong, Z.G. Chen, Q.W. Tian, T.Y. Cao, C.J. Xu, F.Y. Li, Anal. Chem. 81 (2009) 8687–8694.
[23] C. Wang, L. Cheng, Z. Liu, Biomaterials 32 (2011) 1110–1120.
[24] J. Shen, L. Zhao, G. Han, Adv. Drug Deliv. Rev. 65 (2013) 744–755.
[25] Q.i.C. Sun, H. Mundoor, J.C. Ribot, V. Singh, I.I. Smalyukh, P. Nagpal, Nano Lett. 14 (2014) 101–106.
[26] B. Kmella, L. Abranko, P. Fodora, S. Lehotay, J. Food Addit. Contam. 27 (2010) 1415–1430.
[27] L. Parejaa, V. Cesio, H. Heinzen, A. Fernandez-Alba, Talanta 83 (2011) 1613–1622.
[28] S.J. Lehotay, K.A. Son, H. Kwon, U. Koesukwiwata, W. Fu, K. Mastovska, E. Hoh, N. Leepipatpiboon, J. Chromatogr. A 1217 (2010) 2548–2560.
[29] G. Pan, B. Zu, X. Guo, Y. Zhang, C. Li, H. Zhang, Polymer 50 (2009) 2819–2825.
[30] J. Matsui, Y. Miyoshi, O. Doblhoffdier, T. Takeuchi, Anal. Chem. 67 (1995) 4404–4408.
[31] Z. Cheng, P. Ma, Z. Hou, W. Wang, Y. Dai, X. Zhai, J. Lin, Dalton Trans. 41 (2012) 1481–1489.
[32] M. Yu, J. Lin, Z. Wang, J. Fu, S. Wang, H.J. Zhang, Y.C. Han, Chem. Mater. 14 (2002) 2224–2231.
[33] P.P. Yang, Z.W. Quan, L.L. Lu, S.S. Huang, J. Lin, Biomaterials 29 (2008) 692–702.
[34] M.L. Pang, J. Lin, M. Yu, J. Solid State Chem. 177 (2004) 2237–2241.
[35] M. Yu, J. Lin, J. Fu, H.J. Zhang, Y.C. Han, J. Mater. Chem. 13 (2003) 1413–1419.
[36] K. Yoshimatsu, K. Reimhult, A. Krozer, K. Mosbach, K. Sode, L. Ye, Anal. Chim. Acta 584 (2007) 112–121.
[37] H. Wei, Y. Wang, E. Song, Acta Chim. Sin. 69 (2011) 2039–2047.
[38] A. Huignard, V. Buissette, A.C. Franville, T. Gacoin, J.P. Boilot, J. Phys. Chem. B 107 (2003) 6754–6759.
[39] C. Fernyhough, A.J. Ryan, G. Battaglia, Soft Matter 5 (2009) 1674–1682.
[40] H.F. Wang, Y. He, T.R. Ji, X.P. Yan, Anal. Chem. 81 (2009) 1615–1621.
[41] Q. Zhao, X. Rong, L. Chen, H. Ma, G. Tao, Talanta 114 (2013) 110–116.
[42] H. Li, Y. Li, J. Cheng, Chem. Mater. 22 (2010) 2451–2457.
[43] S. Boonpangrak, M.J. Whitcombe, V. Prachayasittikul, K. Mosbach, L. Ye, Biosens. Bioelectron. 22 (2006) 349–354.
[44] J. Pan, H. Hang, X. Dai, J. Dai, P. Huo, Y. Yan, J. Mater. Chem. 22 (2012) 17167–17175.
[45] W.R. Ware, J. Phys. Chem. 66 (1962) 455–458.
[46] X. Hu, Z. Yu, R. Liu, Spectrochim. Acta A 108 (2013) 50–54.
[47] H.J. Zo, J.N. Wilson, J.S. Park, Dyes Pigm. 101 (2014) 38–42.